Dimensional Analysis of Shear Stress of Blood Flow through a Bifurcation: Skin Friction Coefficients

Koonlaya Kanokjaruvijit[1*] and Jirasak Siripokharattana[2]

[1]Department of Mechanical Engineering, the Faculty of Engineering, Naresuan University Phitsanulok, 65000 Thailand
[2]The Faculty of Engineering and Technology, King Mongkut's University of Technology North Bangkok, Rayong Campus
[*] Corresponding author. E-mail address: koonlaya@gmail.com

Abstract

The purpose of the current work is to numerically study blood flow through a bifurcation in a model by using the finite element method. The calculated results are reported in terms of velocity contours, wall shear stress and skin coefficients for specific locations during a pulse cycle such as the peak systole and the diastole, for which the corresponding Reynolds numbers are 750 and 300, respectively. Three types of fluids were examined: blood using the Carreau-Yasuda model, water and air. The shapes of the wall shear stress and skin friction coefficient distributions were similar in all fluid types. However, values of skin friction coefficients for the three fluids were similar, and gave much lower percentage differences between the blood and both Newtonian fluids than wall shear stress values.

Keywords: Bifurcation, Carreau-Yasuda, Dimensional Analysis, Skin Friction Coefficient, non-Newtonian

Introduction

Bifurcation arteries are prone to atherosclerosis, and have been of particular interest for many researchers since drug-eluting stents were invented in the early 2000s. One of the important mechanosensors related to the disease is wall shear stress (WSS), which is likely to modulate endothelial cell functions. The temporal and spatial variations in wall shear stress, including the flow patterns, also play important roles (Fisher, Chien, Barakat, & Nerem, 2001, pp. L529-L533). In addition, wall shear stress is one form of biochemical force, which is a determinant of the endothelial cell function. It adjusts the artery diameter by regulating the production of vasoactive mediators (Reneman, Arts, & Hoeks, 2006, pp. 251-269). With very high wall shear stress, the vessel wall is prone to the platelet thrombosis causing total occlusion. However, intimal thickening may occur if the wall shear stress becomes abnormally low (Ku, 1997, pp. 399-434). Hence, information on wall shear stress is crucial, and needs to be determined. Nonetheless, the wall shear stress cannot be measured directly, and needs to be derived from velocity profiles and blood viscosity data. There have been investigations on blood flow using several approaches, such as *in vivo* (real blood vessel) and *in vitro* (physical model) experiments, numerical analysis using real MRI data and numerical analysis using idealised geometry.

Over the last two decades, *in vivo* investigation methods have changed. In the past, wall shear stress was calculated using the product of blood viscosity and the ratio of the blood velocity and the internal vessel diameter obtained from echo-Doppler examination (Gnasso, et al., 1997, pp. 993-998) or Doppler guide wire (Doucette, et al., 1992, pp. 1899-1911). Nowadays, the 4D MRI method (Harloff, et al., 2003, pp. 3361-3369; Harloff, & Markl, 2012, pp. 137-138) is more common. This is very powerful and more convenient as it shows a realistic model of the blood vessels together with the flow. However, comparisons of *in vivo* flow

results in a bifurcation to that of *in vitro* were found to be in good agreement (Doucette, et al., 1992, pp. 1899-1911; Ku, et al., 1985a). Thus, *in vitro* experiments present reliable wall shear stress information. Many researchers have been conducting *in vitro* blood flow research using either realistic (Ku, et al., 1985b; Davies, Remuzzi, Gordon, Dewey, & Gimbrone, 1986, pp. 2114-2117; Perktold, et al., 1998, pp. 217-228; Botnar, et al., 2000, pp. 137-144; Shuib, Hoskins, & Easson, 2010, pp. 100-104) or geometric bifurcation models (Doucette, et al., 1992, pp. 1899-1911; Ji, Lee, & Lee, 2007, pp. 89-95; Caro, et al., 1996, pp. 185-197; Gijsen, van de Vosse, & Janssen, 1999a, pp. 601-608; Gijsen, van de Vosse, & Janssen, 1999b, pp. 705-713; Yang, Wen, & Tseng, 2008, pp. 2455-2462; Sinnott, Cleary, & Prakash, 2006) using either blood or substitute liquids, whose properties such as viscosity and density are similar to those of blood. In addition, computational simulation has also been conducted in parallel to *in vitro* experiments Botnar, et al., 2000, pp. 137-144; Shuib, et al., 2010, pp. 100-104; Gijsen, et al., 1999a, pp. 601-608; Gijsen, et al., 1999b, pp. 705-713).

One of the main problems in *in vitro* studies of blood flow is the complication of experimental setup. In addition, prior to conducting the experiments, the researchers must obtain permission from the ethical review committee for research in human or animal subjects. Simulated models are obtained either from realistic models such as magnetic resonance images (Perktold, et al., 1998, pp. 217-228; Botnar, et al., 2000, pp. 137-144; Sinnott, et al., 2006; Long, et al., 2000, pp. 229-311; Zhao, et al., 2000, pp. 975-984) or from geometric models (Settler, Niederer, & Anliker, 1981, pp. 145-164; Perktold, Kenner, Hilbert, Spork, & Florian, 1988, pp. 24-31; Xu, & Collins, 1990, pp. 205-215; Chen, & Lu, 2004, pp. 1899-1911; Chen, & Lu, 2006, pp. 818-832; Boyd, Buick, & Green 2007, p. 093103; Siddiqui, Verma, Mishra, & Gupta, 2009, pp. 1-10; Taylor, Hughes, & Zarins, 1998, pp. 155-196). Ku (1997, pp. 399-434) emphasized the flow in carotid and left coronary artery bifurcations, which are prone to shear stress variation and thus atherosclerosis. Thus, many studies have been on the carotid artery (Gnasso, et al., 1997, pp. 993-998; Harloff, et al., 2003, pp. 3361-3369; Harloff, & Markl, 2012, pp. 137-138; Ku, Giddens, Phillips, & Strandnee, 1985a, pp. 13-26; Ku, Giddens, Zarins, & Glagov, 1985b, pp. 293-302; Botnar, et al., 2000, pp. 137-144; Gijsen, et al., 1999a, pp. 601-608; Zhao, et al., 2000, pp. 975-984; Settler, et al., 1981, pp. 145-164), and presented similar results on skewed velocity profiles towards the inner wall of the internal carotid sinus (the bigger branch). In addition, non-Newtonian effects have been brought in to consideration by several researchers, i.e. the Carreau-Yasuda shear thinning model (Gijsen, et al., 1999a, pp. 601-608; Chen, & Lu, 2004, pp. 1899-1911; Chen, & Lu, 2006, pp. 818-832; Boyd, et al., 2007, p. 093103) and the Casson model (Shuib, et al., 2010, pp. 100-104; Siddiqui, et al., 2009, pp. 1-10), which take the red blood cells into consideration in the hematocrit form.

Gijsen, et al. (1999a, pp. 601-608) performed both *in vitro* experiments and numerical studies on the non-Newtonian effects of blood flow through a carotid bifurcation by closely investigating axial velocity distributions of the cross sections along the common carotid artery and the internal carotid artery (larger branch vessel). They also took various geometric factors into consideration that influence the velocity profiles such as the curvature effect, the change of the cross-sectional area and

the presence of a shear layer. The non-Newtonian behaviour revealed through the axial velocities showed a flatter profile and the peak shifted towards the inner wall compared to that of the Newtonian. Later, they numerically studied the detail of pulsed blood flow through a 90° curved tube (Gijsen, et al., 1999b, pp. 705-713) using the Carreau-Yasuda model compared to the Newtonian model to closely investigate the secondary flow. The difference in the axial velocity profiles obtained from both models became pronounced downstream of the tube, and was explained by the fact that the secondary flow for the non-Newtonian fluid had developed more slowly. In addition, the numerical results were compared to the experimental results using xanthan gum solution, and good agreement was found.

Chen, & Lu (2004, pp. 1899-1911; 2006, pp. 818-832) examined a geometric bifurcation model with one non-planar curve branch with a 90 degree bifurcation angle using the Carreau-Yasuda model compared with the Newtonian one using the finite element method, and presented the results in terms of the axial velocity profiles and the wall shear stress distributions at different locations in the bifurcation. They found that the non-Newtonian effect became pronounced downstream of both branches, and the strong flow from the outer wall towards the inner wall caused counter-rotating vortices due to a centripetal acceleration produced by the curvature in the straight branch. In addition, in the non-planar curve branch, asymmetric flow patterns were found due to the bending effect of the tube.

From the aforementioned literature, haemodynamic researchers have shown attempts to find more convenient and less costly ways to examine the detail of blood flow inside blood vessels to avoid handling complicated experimental setups. Thus, in the present study, the flow of three fluids, blood using Carreau-Yasuda model, water and air in an artery bifurcation is numerically investigated using the finite element method at the peak systole and the diastole. The results are reported as velocity contours, wall shear stress values and skin friction coefficients for all fluids. The latter part of the study is aimed to determine whether air could potentially substitute blood, so that future *in vitro* experiments could be less complicated and less expensive.

Research Methods

The 3D solver and meshing programme, COMSOL, was used throughout this study. Three types of fluids were numerically simulated: blood, water and air. All fluid flows were assumed steady incompressible and laminar in a three-dimensional bifurcation model. The finite element method was used throughout this research with a tolerance of 10^{-6}. The mean axial velocities of the pulse flow were derived using data from Gijsen, et al. (1999a, pp. 601-608), which gave Reynolds numbers at the entrance of 750 and 300 for the peak systole and the diastole, respectively.

1. Computational Domain

Figure 1 shows the geometry and the dimensions of the bifurcation tested in this research. The diameter of the main vessel was 4 mm with length 30 mm. The diameters of the branch vessels were 3.2 mm and 3.1 mm with lengths of 19 mm and 17 mm, respectively and a bifurcating angle of 45°. These values come from left-circumflex artery data presented by Dodge, Brown, Bolson, & Dodge. (1992, pp. 232-246). The vessel walls were assumed thin and rigid, and thus the velocity conditions follow the no-slip condition and with no penetration constraints on the walls. Results in terms of velocity contours, shear stress and skin friction coefficient distributions from the selected cross

sections at different locations (Figure 2) are presented. The cross section A-A′ in the main vessel was 6 diameters away from the entrance. Three cross sections, B-B′, C-C′ and D-D′ at the bifurcation junction were selected in order to show changes in the flow when the cross sectional areas changes. Along each branch vessel, the cross section at the beginning of the vessel (L1-L1′ for the branch vessel of diameter 3.2 mm and S1-S1′ for that of 3.1 mm) as well as that at the mid vessel (L2-L2′ and S2-S2′) have been selected.

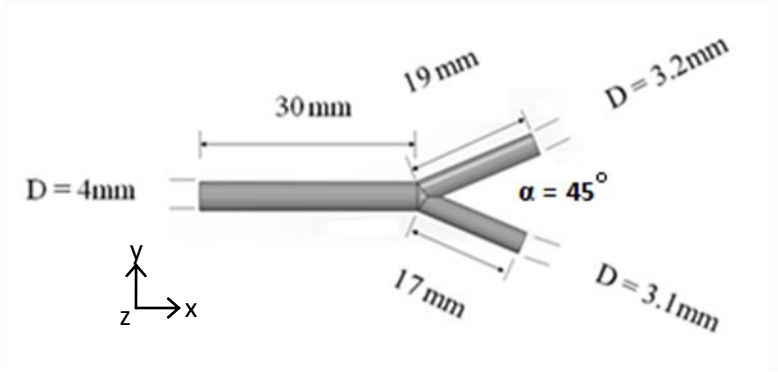

Figure1 Computational domain and dimensions

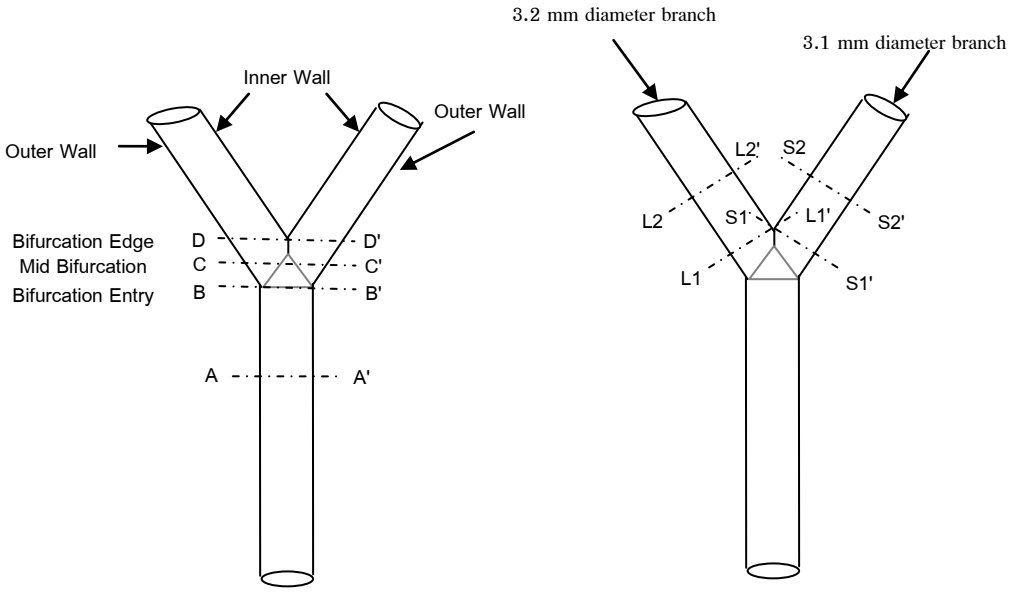

Figure 2 Cross sections and nomenclature at different locations at the bifurcation (not to scale).

2. Governing Equations

The governing equations for this study is the steady three-dimensional Navier-Stokes, which contains the continuity equation and the x-, y- and z-momentum equations in the form that is more convenient to define the non-Newtonian viscosity and the importance of shear rate as

$$\nabla \cdot \boldsymbol{u} = 0 \qquad (1)$$

$$\rho(\boldsymbol{u}\nabla\boldsymbol{u}) = \nabla P + \nabla \cdot \boldsymbol{T} \qquad (2)$$

where **T** is the stress tensor, which depends on the deformation tensor **D** as $\boldsymbol{T} = 2\mu\dot{\gamma}\boldsymbol{D}$, and $\boldsymbol{D} = \frac{1}{2}(\nabla\boldsymbol{u}+\nabla\boldsymbol{u}^T)$. Note that for Newtonian fluids such as water and air their viscosities, μ, are constant whereas that of the blood varies with the shear rate due to the shear thinning behavior by the microscopic activities of red blood cells such as aggregation, deformation and alignment (Chen, & Lu, 2004, pp. 1899-1911). The viscosities for water and air were 695×10^{-6} N-s/m^2 and 189.32×10^{-7} N-s/m^2, respectively, and obtained at 37°C in accordance to human normal body temperature.

For blood flow, the Carreau-Yasuda shear thinning model is applied as shown in Equation (3) with the parameters and constants given by Gijsen, et al. (1999a, pp. 601-608; 1999b, pp. 705-713),

$$\mu = \mu_\infty + (\mu_0 - \mu_\infty)[1 + (\lambda\nabla\boldsymbol{u})^a]^{\frac{n-1}{a}} \qquad (3)$$

where μ_∞ is the viscosity of the blood when the infinite shear applies = 2.2×10^{-3} Pa-s

μ_0 is the viscosity of the blood when the minimum shear applies = 22×10^{-3} Pa-s

λ is the characteristic time constant = 0.110 s

n = 0.392

a = 0.644

Note that the properties of all fluids used throughout this study are at 37°C. The parameters λ, n and a control the behavior of the non-Newtonian blood, and can be obtained from curve fitting. Hence, the values may vary depending on the data the researchers have.

3. Boundary Conditions

The velocities of steady blood flow through a bifurcation were obtained from Reynolds number data used by Gijsen, et al. (1999a, pp. 601-608). For the peak systole, the Reynolds number was 750 and the diastole Reynolds number was 300. Hence, the entrance velocity at the main vessel could be calculated for both cases. The exit boundary condition of the branch vessels were set to ambient pressure. In addition, the vessel walls were assumed rigid thus the no-slip condition was applied.

4. Mesh Generation

A tetrahedral element mesh was generated throughout the vessels using the Delaunay algorithm with the boundaries partitioned into triangular elements. A mesh density dependence check was carried out. Fig.3 shows the concurrence of the velocity distributions at the cross-sections of the parent vessel for mesh densities of 8.424, 31.391 and 96.023 elements/mm^3 for blood flow using the Carreau-Yasuda model. Computational times for each mesh density were 13.01, 67.349 and 325.25 seconds, respectively. Slight differences were found at the mid plane and between r/R = 0.2 and 0.4. However, for 3D meshes, higher mesh density does not necessarily always mean more accurate results, but usually requires more computational memory and increased solution convergence time. According to the study by Holzbecher, & Si (2008), higher mesh density did not always lead to an improvement in accuracy. In the current study, a problem of divergence of some points on some elements were found for the mesh density of 96.0226 elements/mm^3. Therefore, in this study, a mesh density of 31.391 elements/mm^3 was chosen as a compromise between accuracy and convergence.

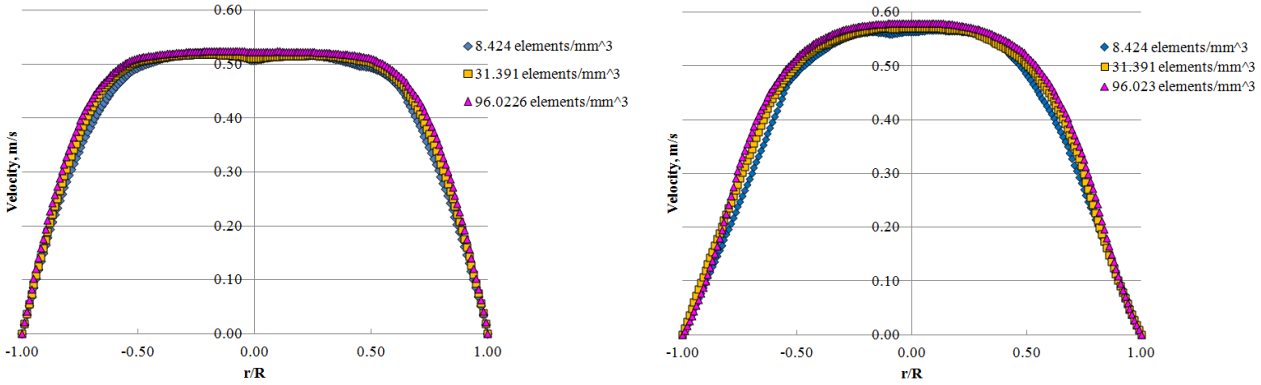

(a) Mid parent vessel (b) End parent vessel

Figure 3 Axial velocity distribution in the parent vessel for blood flow at peak systole (Re = 750) for different mesh densities at different locations.

5. Data Reduction

Since the wall shear stress cannot be measured directly, the velocity values at 0.1 mm from the vessel wall were taken and brought into the calculation of wall shear rate, $\dot{\gamma}$, as shown in the following Eq. (4)

$$\dot{\gamma} = \left.\frac{du_r}{dr}\right|_{\text{wall}} \tag{4}$$

where u_r is the circumferential velocity and r is the radial direction. The viscosity for blood was calculated using Eq.(3) and the constant viscosities for water and air were obtained. The product of the viscosity and wall shear rate at the same location gave the wall shear stress (WSS or τ_w). Finally, the skin friction coefficient, C_f, was calculated according to the following definition

$$C_f = \frac{\text{WSS}}{\frac{1}{2}\rho U^2} \tag{5}$$

where U is the average velocity in each vessel.

Results and Discussion

Figure 2 shows locations at the main and branch vessels, where the cross sections were selected to present the results of velocity contours, wall shear stress and skin friction coefficient. The results at the peak systole and the diastole were examined.

1. Velocity Contours

1.1 Peak Systole

Figure 4 shows the velocity contours of the blood flow at various cross sections along the main vessel and the bifurcation. The cross section A-A′ presents normal flow in a straight pipe with flattened velocity profiles in the central vicinity. At the beginning of the bifurcation, section B-B′, the contours begin to become slightly elliptical in shape indicating the starting point of the flow dividing into two branches. This becomes more pronounced nearer the bifurcation cusp in sections C-C′ and D-D′.

The flow along each branch vessels shows similarity in the velocity contour for either cross section as exhibited in Figs.5 and 6. The velocities are skewed to the inner wall showing crescent or C-shaped contours, which correspond to the secondary flow pattern (Gijsen, et al., 1999a,

pp. 601-608). Once the flow is divided by the apex of the bifurcation, the cross sectional area increases by approximately 24% and so the average flow velocity reduces. The high momentum flow at the central vicinity of the vessel moves towards the inner wall, and is replaced by the lower momentum fluid from the outer wall. Then, the fluid at the inner wall moves peripherally towards the outer wall. This behavior could be explained by the tendency for adverse axial pressure gradients to develop, as described by Chen and Lu (2004, pp. 1899-1911).

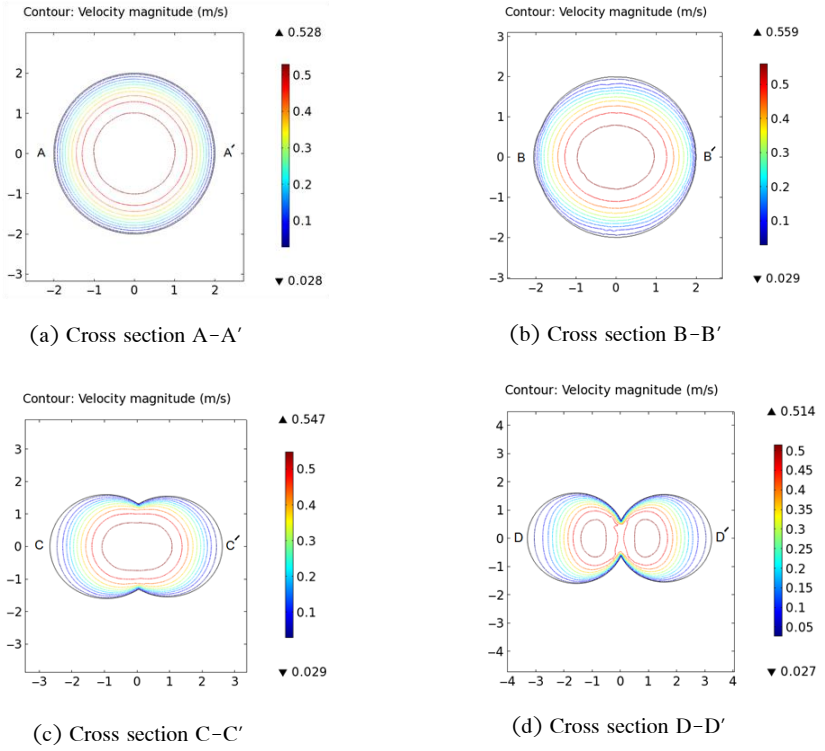

(a) Cross section A-A′ (b) Cross section B-B′

(c) Cross section C-C′ (d) Cross section D-D′

Figure 4 Velocity contours in the main vessel and the bifurcation junction at peak systole (Re = 750).

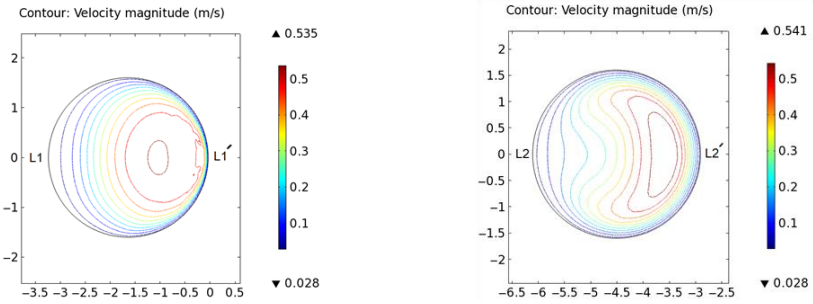

(a) Cross section L1-L1′ (b) Cross section L2-L2′

Figure 5 Velocity contours in the 3.2 mm branch vessel at peak systole.

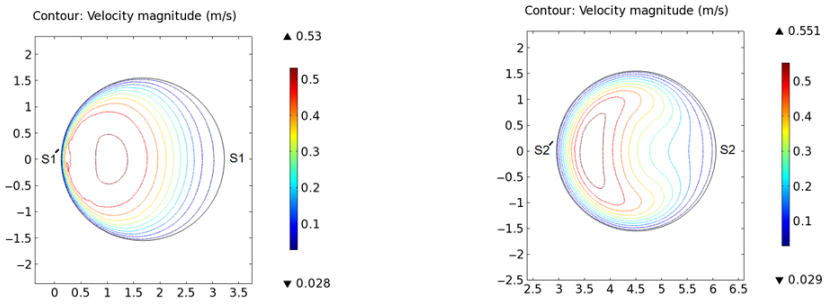

(a) Cross section S1–S1′ (b) Cross section S1–S1′

Figure 6 Velocity contours in the 3.1 mm branch vessel at peak systole.

1.2 Beginning of Diastole and End of Diastole

The flow velocities at the beginning and the end of diastole are similar and therefore the Reynolds number of 300 was used for both instances. Figure 7 shows similar contour shapes to those of the peak systole in Figure 4. However, the skewness to the inner wall is less severe for the cross section L2–L2′. This is thought to be because the flow contains less momentum than that of the peak systole. Thus, the aforementioned adverse pressure gradient was less acute, and the degree of fluid replacement became less severe.

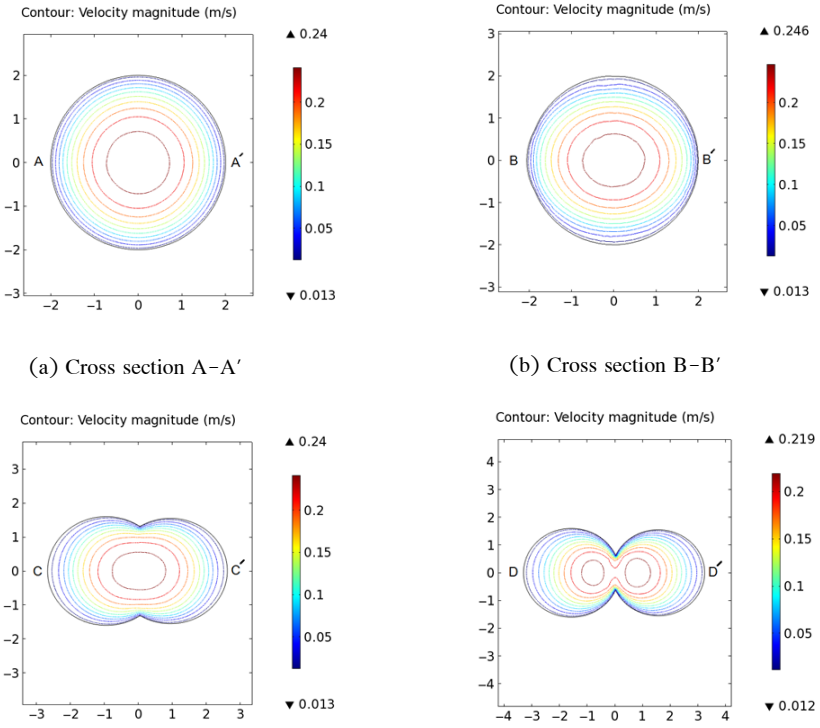

(a) Cross section A–A′ (b) Cross section B–B′

(c) Cross section C–C′ (d) Cross section D–D′

Figure 7 Velocity contours in the main vessel and the bifurcation junction at diastole (Re = 300).

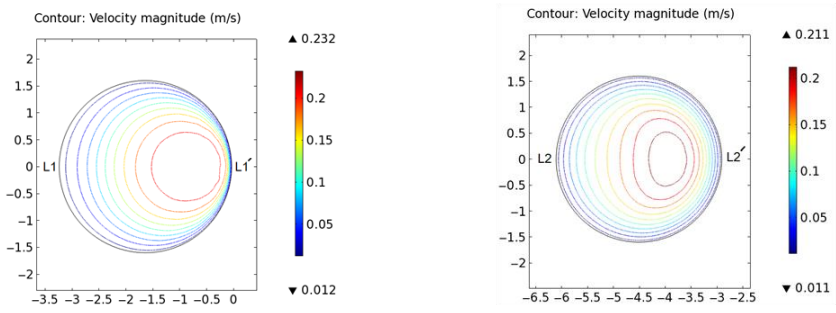

(a) Cross section L1-L1′ (b) Cross section L2-L2′

Figure 8 Velocity contours in the 3.2 mm branch vessel at diastole.

2. Wall Shear Stress (WSS)

The wall shear stress values vary circumferentially around the vessel. The locations are shown in Figure 9. Values for the main vessel and the branch vessels after the bifurcation edge are shown in Figure 9(a), and those with cusped parts in the bifurcation junction in Figure 9(b). For example, 0^{o} or 360^{o} represents the inner wall of the 3.2 mm diameter branch vessel (see Figure 2), and 180^{o} the outer wall. For the 3.1 mm diameter vessel, 0^{o} or 360^{o} is the outer wall, and 180^{o} the inner wall. For either branch, 90^{o} represents the posterior side (of the human body) and 270^{o} the anterior.

Figure 10 shows the wall shear stress of the main vessel for the three fluids at the peak systole. It shows that the blood flow gives significantly higher wall shear stress than the water and the air by 93.07% and 95.59% on average, respectively. The differences are due to the shear thinning effect of the blood. The wall shear stress distributions shown in Fig.11 at cross sections B-B′, C-C′ and D-D′ of the bifurcation exhibit similar patterns. At the beginning of the bifurcation, B-B′, secondary peaks are present at 0^{o} and 180^{o}, with the minima located at the posterior and the anterior. At the cross section C-C′, the peaks are found at 90^{o} and 270^{o}, where the cusped regions cause acceleration of the fluid as it begins to divide into the two branch vessels. The minima in this case are at 0^{o} and 180^{o}. At the bifurcation edge, D-D′, where the flow splits, the cusps are closer than those at the C-C′ section, and thus higher wall shear stress values are found. The maxima and the minima are also seen at the same positions as those of the C-C′ section.

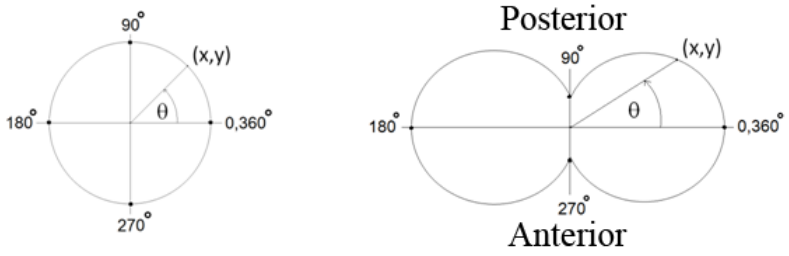

(a) Straight duct (b) Junction

Figure 9 Peripheral locations of the vessel cross section.

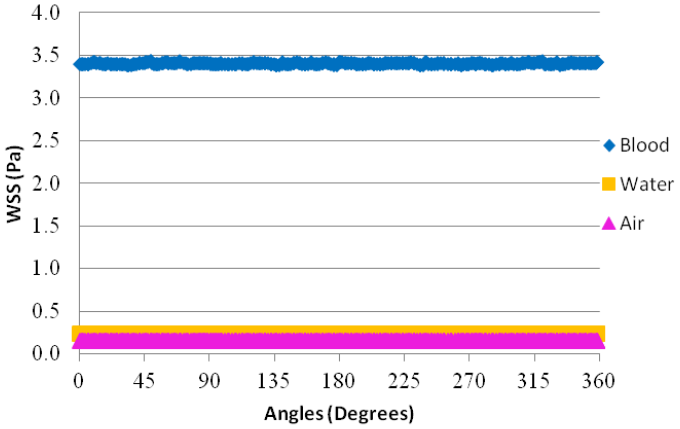

Figure 10 Wall shear stress in the main vessel for the three fluids at peak systole.

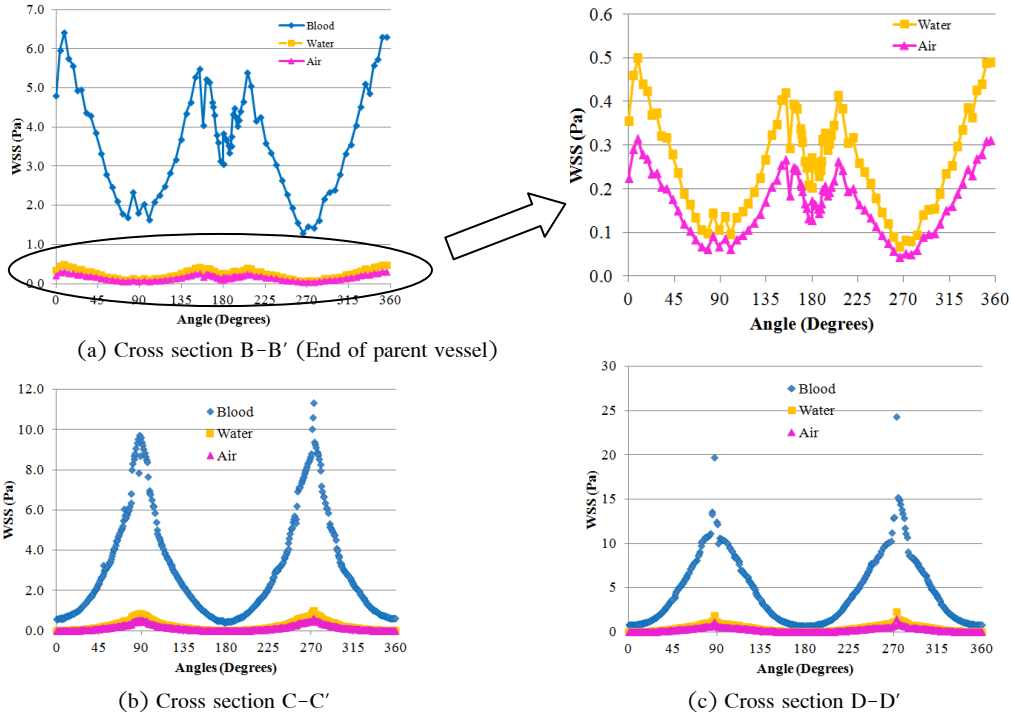

(a) Cross section B–B′ (End of parent vessel)

(b) Cross section C–C′

(c) Cross section D–D′

Figure 11 Wall shear stresses at the bifurcation junction for the three fluids at peak systole.

The wall shear stress of the flow through the branch vessels is illustrated in Figure 12. High wall shear stress is found near the inner wall (0°) at the entry and mid vessel. This corresponds with the skewness of the flow towards the inner wall seen in Figure 5. However, lower wall shear stress is found at the outer wall (180°). Further downstream, i.e. at L2–L2′, the wall shear stress is significantly reduced, on average by 45% compared to that of the cross section L1–L1′. This is due to a higher momentum transfer towards the inner wall upstream.

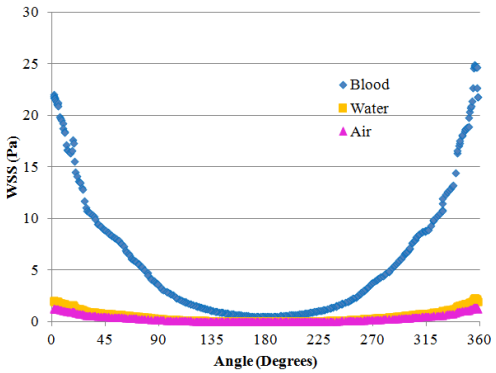

(a) Cross section L1-L1′

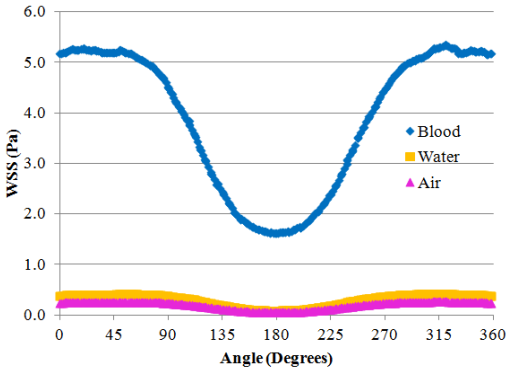

(b) Cross section L2-L2′

Figure 12 Wall shear stress in the 3.2 mm branch vessel for the three fluids at peak systole. Similar wall shear stress patterns are observed in the 3.1 mm diameter branch vessel.

3. Skin Friction Coefficients (C_f)

The skin friction coefficient is derived from the value of the wall shear stress according to Equation (5). Figure 13 shows the constant linear trend lines for all three fluids at the cross section A-A′ in the main vessel at peak systole with an average skin friction coefficient of 3.247×10^{-2} for the blood and 2.69×10^{-2} for both water and air. The difference between the average values of skin friction coefficient of non-Newtonian and Newtonian fluids is 5.6×10^{-2}, a percentage difference of approximately 17%. Note that this difference is far lower than that for the wall shear stress. Moreover, the difference in the skin friction coefficient values of the Newtonian fluids is minuscule compared to the 36.63% difference for the wall shear stress.

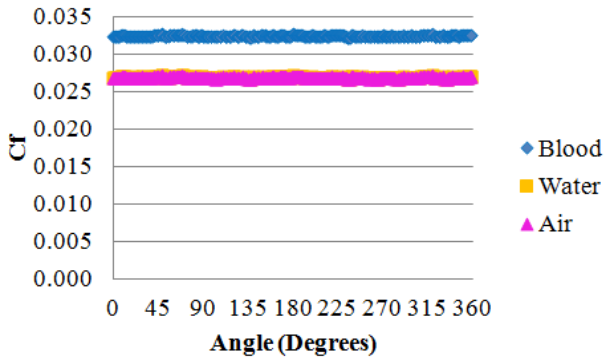

Figure 13 Comparison of skin friction coefficients of the three fluids in the main vessel at peak systole

The skin friction coefficient distributions at cross sections B-B′, C-C′ and D-D′ in the bifurcation are exhibited in Figure 14. These are similar in shape to those of the wall shear stress (Figure 11). However, the values of wall shear stress differ greatly between non-Newtonian and Newtonian fluids. However, when considering the local percentage difference between either blood and water or blood and air, $(C_{f,blood} - C_{f,water/air})/C_{f,blood} \times 100$ (Figure 15),

the trends are opposite to those of the skin friction coefficient distributions, i.e. at the peaks in skin friction coefficient, the minimum percentage differences between the skin friction coefficient values of the blood and both Newtonian fluids are seen, and vice versa. This is probably due to the fact that the value of the denominator of the percentage difference is very low, even though the difference is quite low. At 0^{o} of the cross section B-B′, the maximum peak in Figure 14(a) shows a skin friction coefficient value of 0.06 whereas the corresponding percentage difference in Figure 15(a) is only 8%. However, at 180^{o}, and at the posterior (90^{o}) and anterior (270^{o}) walls, the skin friction coefficient values are just 0.02, 0.01 and 0.008, respectively, but the percentage differences jump to 22%, 32% and 38%, respectively. The skin friction coefficient and the percent difference distributions for cross sections C-C′ and D-D′ also present similar trends to those of B-B′.

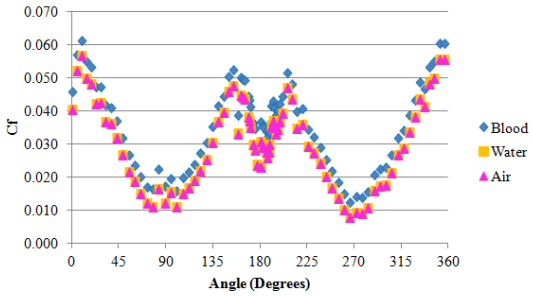

(a) Cross section B-B′

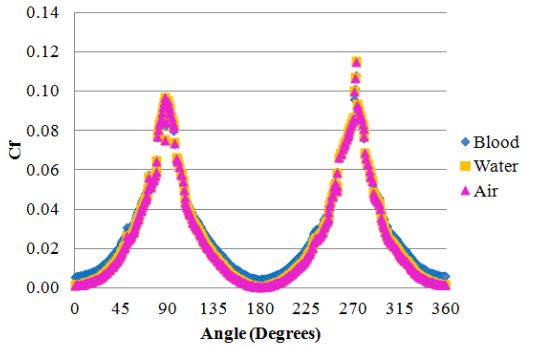

(b) Cross section C-C′

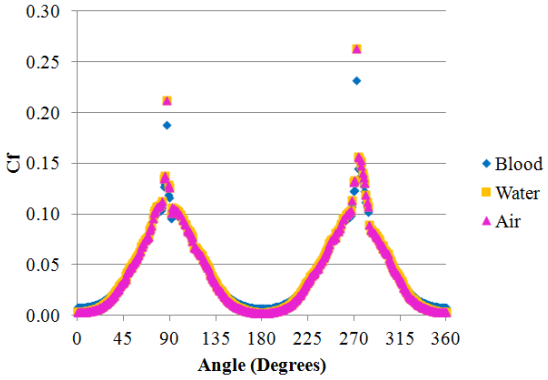

(c) Cross section D-D′

Figure 14 Skin friction coefficients of the three fluids at various cross sections in the bifurcation at peak systole.

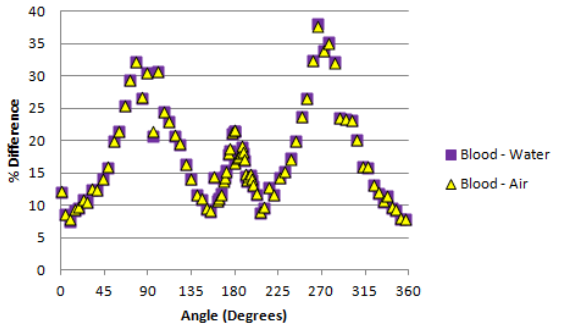

(a) Cross Section B-B′

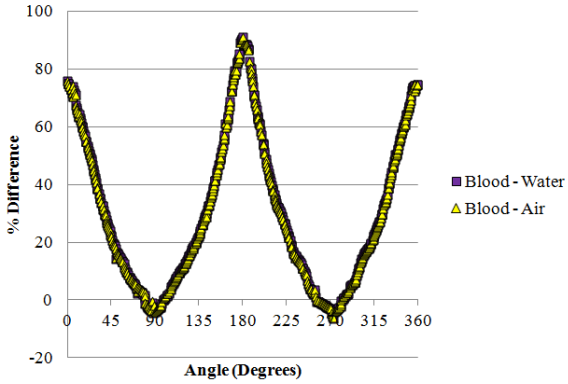

(b) Cross Section C-C′

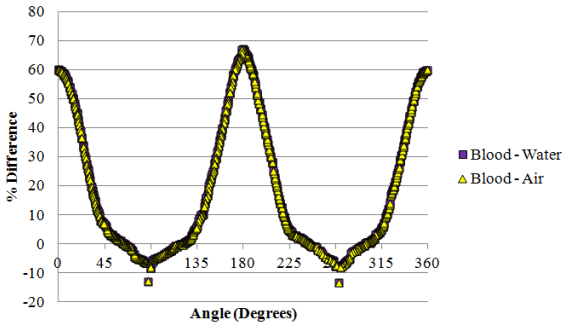

(c) Cross Section D-D′

Figure 15 Percentage difference in skin friction coefficients of non-Newtonian and Newtonian fluids at various cross sections in the bifurcation at peak

Figure 16 exhibits skin friction coefficient distributions for the cross sections at the beginning and middle of 3.2 mm diameter branch vessel showing the maximum and the minimum peaks at the inner and outer walls, respectively. A deeper comparison of skin friction coefficient values can be made for the wall shear stress values for both cross sections. The skin friction coefficient curves for all three fluids for the cross section L1-L1′ display the same trend, as shown in Figure 16(a). The percentage difference in values is 82% at the outer wall shown in Figure 17(a) whereas the inner wall shows a -7% difference. Figure 16(b) shows the skin friction coefficient distributions of all

fluids at the cross section L2-L2′ located at the middle of the 3.2 mm diameter branch vessel. Distinct dissimilarities between the skin friction coefficient values for the non-Newtonian and the Newtonian fluids are found in the vicinities of the inner (0^{o}) and the outer walls (180^{o}), where the replacement of the higher momentum fluid from the central region of the vessel to the inner wall and that from the inner wall towards the outer wall takes place as described earlier. However, the percentage differences in Figure 17(b) show good agreement between the blood and both Newtonian fluids.

Thus far, if the calculated values for skin friction coefficient to be believed, air could be considered a potential replacement for blood in an *in vitro* experiment simulating blood flow through a bifurcation. This would greatly simplify the experimental setup. Nonetheless, the percentage difference between the skin friction coefficients of the blood and air means that the final results should be adjusted accordingly.

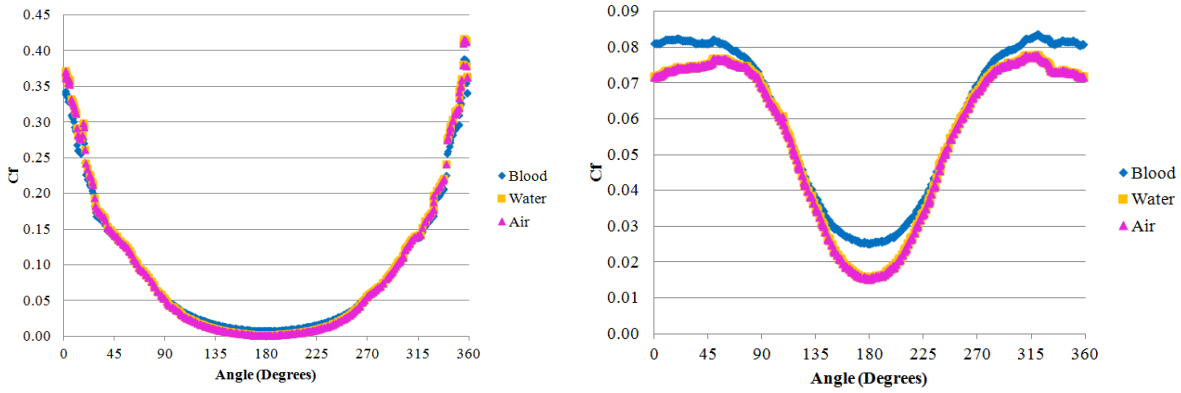

(a) Cross section L1-L1′ (b) Cross section L2-L2′

Figure 16 Skin friction coefficients of the three fluids for the branch vessel at systole.

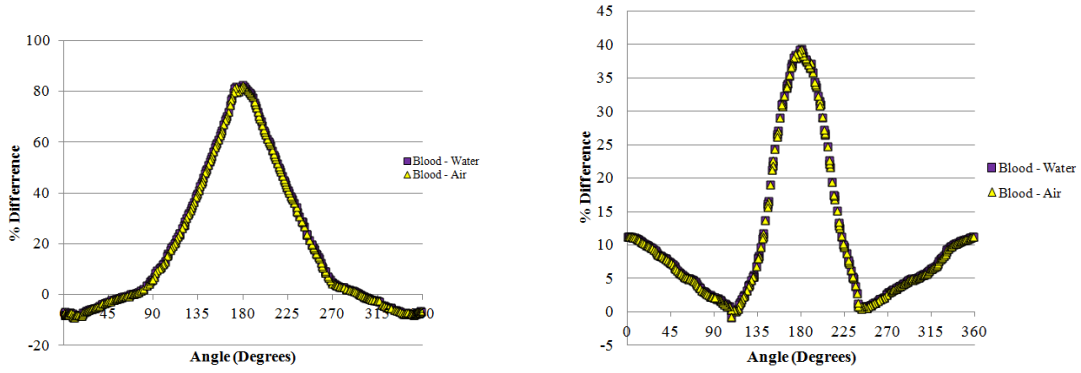

(a) Cross section L1-L1′ (b) Cross section L1-L1′

Figure 17 Percentage difference in skin friction coefficients between non-Newtonian and Newtonian fluids at the branch vessel at peak systole.

4. Validation

The dimensionless velocity profiles were validated against those obtained from the literature. The cross section at 6D (A-A') from the entry of the main branch was selected, so that the entry region and the flow division would have least influence. Figure 18 shows a comparison of the data from the current study to those from Gijsen, et al. (1999b, pp. 705-713), who used the Carreau-Yasuda model with a finite element method in a straight tube for Re = 200. Good agreement was found. The Lattice Boltzman method with the Carreau-Yasuda model was employed by Boyd, et al. (2007, p. 093103). A comparison with the current study (Figure 19) shows differences in the vicinity away from the wall. Figure 20 displays a comparison of the dimensionless velocity profiles of the current study at Re = 200 to those of Taylor, et al. (1998, pp. 155-196) at peak systole with an unreported Reynolds number. They agree surprisingly well despite the fact that Taylor, et al. (1998, pp. 155-196) used the Newtonian fluid with the Womersley velocity profile.

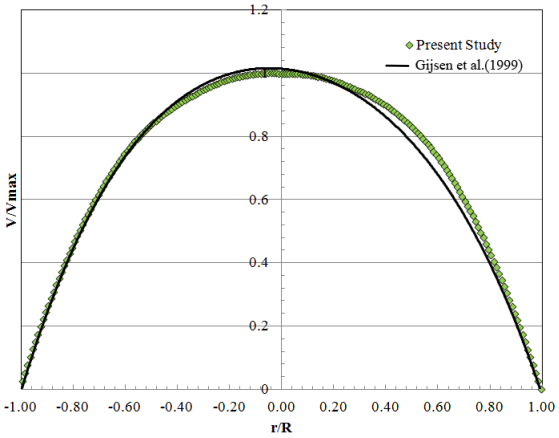

Figure 18 Comparison of dimensionless velocity profile of the current study to that of Gijsen, et al. (1999b) at Re = 270.

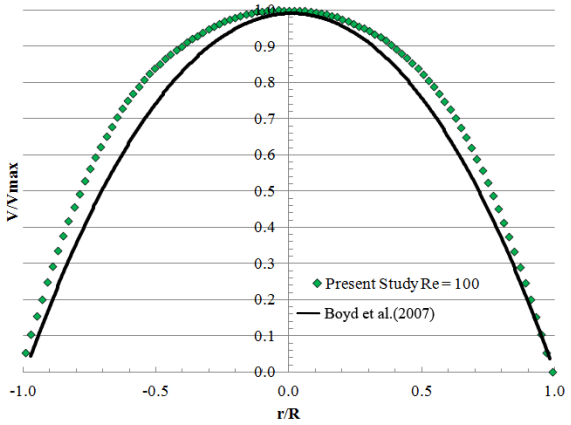

Figure 19 Comparison of dimensionless velocity profiles at Re = 100 of the present study to that of Boyd, et al. (2007, p. 093103).

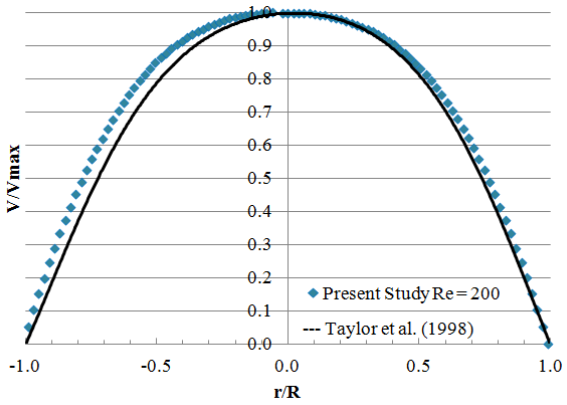

Figure 20 Comparison of dimensionless velocity profiles at Re = 200 of the current study to that of Taylor, et al. (1998, pp. 155-196).

Conclusions

Flow through a bifurcation is numerically investigated by using three fluids: blood simulated using the Carreau-Yasuda model, water and air. Velocity contours, wall shear stress and skin friction coefficients are presented consecutively. The velocity contours at different cross sections show changes along the bifurcation. A skewness in velocity values towards the inner wall is present downstream of each branch vessel. This was explained by the replacement of high momentum fluid from the central part of the branch vessel to that at the inner wall, and the fluid at the inner wall to lower momentum fluid at the outer wall. The wall shear stress distributions of the three fluids exhibit similar trends with the higher values for blood and similar values for water and air. Finally, the skin friction coefficient distributions of the three fluids are in good agreement, except near the vicinities of the inner and outer walls, where the replacement of the high momentum fluid with the low one takes place. However, considering the percentage differences between the skin friction coefficient values of the blood and both Newtonian fluids, which show the greatest differences at the minima but low percentage difference at the maximum peaks. In spite of this, the Newtonian fluid, especially air, is thought to be a potential substitute fluid for blood in an *in vitro* experiment with a careful report of error. Nevertheless, other parameters related to the oscillatory nature of a pulse cycle should also be examined in the future.

Acknowledgement

The authors would like to acknowledge that this research has been funded by Naresuan University under the contract number R2558C046. The authors also would like to acknowledge Dr. Aaron Costall and Mr.Paul Mison for proofreading this paper.

References

Botnar, R., Rappitsch, G., Scheidegger, M.B., Liepsch, D., Perktold, K., & Boesiger, P. (2000). Hemodynamics in the carotid artery bifurcation: a comparison between numerical simulation and in vitro MRI measurements. *Journal of Biomechanics, 33*(2), 137-144.

Boyd, J., Buick, J. M., & Green S. (2007). Analysis of the Casson and Carreau-Yasuda non-Newtonian blood models in steady and oscillatory flows using the lattice Boltzmann method. *Physics of Fluids*, 19, 093103.

Caro, C. G., Doorly, D. J., Tarnawski, M., Scott, K.T., Long, Q., & Dumoulin, C. L. (1996). Non-planar curvature and branching of arteries and non-planar-type flow. *Proceedings of the Royal Society of London A.*, 452, 185-197.

Chen, J., & Lu, X-Y. (2004). Numerical investigation of the non-Newtonian blood flow in a bifurcation model with a non-Planar branch. *Journal of Biomechanics*, *37*(12), 1899-1911.

Chen, J., & Lu, X-Y. (2006). Numerical investigation of the non-Newtonian pulsatile blood flow in a bifurcation model with a non-Planar branch. *Journal of Biomechanics*, *39*(5), 818-832.

Davies, P. F., Remuzzi, A., Gordon, E. J., Dewey, Jr., F., & Gimbrone, Jr., M. A. (1986). Turbulent fluid shear stress induced vascular endothelial cell turnover in vitro. *Proceeding of the National Academy of Sciences of the United States of America*, *83*(7), 2114-2117.

Dodge, J. T., Brown, B. G., Bolson, E. L., & Dodge, H. T. (1992). Lumen diameter of normal human coronary arteries. Influence of age, sex, anatomic variation, and left ventricular hypertrophy or dilation. *Circulation*, 86, 232-246.

Doucette, J. W., Corl, P. D., Payne, H. M., Flynn, A. E., Goto, M., & Nassi, M., et al. (1992). Validation of a Doppler guide wire for intravascular measurement of coronary artery flow velocity. *Circulation*, 85, 1899-1911.

Fisher, A. B., Chien, S., Barakat, A. I., & Nerem, R. M. (2001). Endothelial cellular response to altered shear stress. *American Journal of Physiology - Lung Cellular and Molecular Physiology*, 281, L529-L533.

Gijsen, F. J. H., van de Vosse, F. N., & Janssen, J. D. (1999a). The influence of the non-Newtonian properties of blood on the flow in large arteries: steady flow in a carotid bifurcation model. *Journal of Biomechanics*, *32*(6), 601-608.

Gijsen, F. J. H., van de Vosse, F. N., & Janssen, J. D. (1999b). The influence of the non-Newtonian properties of blood on the flow in large arteries: unsteady flow in a 90^{o} curved tube. *Journal of Biomechanics*, 32(7), 705-713.

Gnasso, A., Irace, C., Carallo, C., de Franceschi, M. S., Motti, C., & Mattioli, P. L., et al. (1997). In vivo association between low wall shear stress and plaque in subjects with asymmetrical carotid atherosclerosis. *Stroke*, *28*(5), 993-998.

Harloff, A., Berg, S., Barker, A. J., Schollhorn, J., Schumacher, M., & Weiller, C., et al. (2003). Wall shear stress distribution at the carotid bifurcation: Influence of eversion carotid endarterectomy. *European Radiology*, *23*(12), 3361-3369.

Harloff, A., & Markl, M. (2012). In vivo wall shear stress patterns in carotid bifurcation assessed by 4D MRI. *Perspectives in Medicine*, 1, 137-138.

Holzbecher, E., & Si, H. (2012). *Accuracy tests for COMSOL – and Delaunay meshes.* Proceeding of the COMSOL Conference: Hannover.

Ji, H. S., Lee, J. Y., & Lee, S. J. (2007). In-vitro study on the hemorheological characteristics of chicken blood in microcirculation. *Korea-Australia Rheology Journal, 19*(2), 89-95.

Ku, D. (1997). Blood flow in arteries. *Annual Review of Fluid Mechanics,* 29, 399-434.

Ku, D. N., Giddens, D. P., Phillips, D. J., & Strandnee, Jr., D. E. (1985a). Hemodynamics of the normal human carotid bifurcation: in vitro and in vivo studies. *Ultrasound in Medicine & Biology, 11*(1), 13-26.

Ku, D. N., Giddens, D. P., Zarins, C. K., & Glagov, S. (1985b). Pulsatile flow and atherosclerosis in the human carotid bifurcation – positive correlation between plaque location and low and oscillating shear stress. *Arteriosclerosis, 5*(3), 293-302.

Long, Q., Xu, X. Y., Ariff, B., Thom, S. A., Hughes, A. D., & Stanton, A. V. (2000). Reconstruction of blood flow patterns in a human carotid bifurcation. *Journal of Magnetic Resonance Imaging, 11*(3), 229-311.

Perktold, K., Hofer, M., Rappitsch, G., Loew, M., Kuban, B. D., & Friedman, M. H. (1998). Validated computation of physiologic flow in a realistic coronary artery branch. *Journal of Biomechanics,* 31, 217-228.

Perktold, K., Kenner, T., Hilbert, D., Spork, B., & Florian, H. (1988). Numerical blood flow analysis: arterial bifurcation with a saccular aneurysm. *Basic Research in Cardiology, 83*(1), 24-31.

Reneman, R. S., Arts, T., & Hoeks, A. P. G. (2006). Wall shear stress – an important determinant of endothelial cell function and structure in the arterial system in vivo. *Journal of Vascular Research,* 48(3), 251-269.

Settler, J. C., Niederer, P., & Anliker, M. (1981). Theoretical analysis of arterial hemodynamics including the influence of bifurcation Part I: Mathematical model and prediction of normal pulse pattern. *Annals of Biomedical Engineering, 9*(2), 145-164.

Shuib, A. S., Hoskins, P. R., & Easson, W. J. (2010). Flow regime characterization in a diseased artery model. *World Academy of Science, Engineering and Technology,* 38, 100-104.

Siddiqui, S. U., Verma, N. K., Mishra, S., & Gupta, R. S. (2009). Mathematical modelling of pulsatike flow of Casson′s fluid in arterial stenosis. *Applied Mathematics and Computation, 210*(1), 1-10.

Sinnott, M., Cleary, P. W., & Prakash, M. (2006, December). *An investigation of pulsatile blood flow in a bifurcation artery using a grid-free method.* 5th International Conference on CFD in the Progress Industries CSIRO, Melbourne, Australia.

Taylor, C. A., Hughes, T. J. R., & Zarins, C. K. (1998). Finite element modeling of blood flow in arteries. *Computer Methods in Applied Mechanics and Engineering,* 158, 155-196.

Xu, X. Y., & Collins, M. W. (1990). A review of the numerical analysis of blood flow in arterial bifurcations, Proceedings of the Institution of Mechanical Engineers, Part H. *Journal of Engineering in Medicine*, *204*(4), 205-215.

Yang, A-S., Wen, C-Y., & Tseng, L-Y. (2008). *In vitro* characterization of aortic flow using numerical simulation, phase-contrast magnetic resonance imaging, and particle tracking images, Proceedings of the Institution of Mechanical Engineers. Part C. *Journal of Mechanical Engineering Science*, *222*(12), 2455-2462.

Zhao, S. Z., Xu, X. Y., Hughes, A. D., Thom, S. A., Stanton, A. V., & Ariff, B., et al. (2000). Blood flow and vessel mechanics in a physiologically realistic model of a human carotid arterial bifurcation. *Journal of Biomechanics*, *33*(8), 975-984.